

**International Journal of Mechatronics and Manufacturing Systems**

ISSN online: 1753-1047 - ISSN print: 1753-1039  
<https://www.inderscience.com/ijmms>

---

**On predicting machined part accuracy from CNC machine errors using artificial neural networks**

Marios-Christos Koutsogiannis, George-Christopher Vosniakos

**DOI:** [10.1504/IJMMS.2023.10057692](https://doi.org/10.1504/IJMMS.2023.10057692)

**Article History:**

Received:	15 February 2023
Last revised:	22 May 2023
Accepted:	01 June 2023
Published online:	14 September 2023

---

## On predicting machined part accuracy from CNC machine errors using artificial neural networks

---

Marios-Christos Koutsogiannis  
and George-Christopher Vosniakos\*

School of Mechanical Engineering,  
Manufacturing Technology Laboratory,  
National Technical University of Athens,  
Heron Politehniou 9, 15773, Athens, Greece  
Email: xrhstoskoutsogiannis@gmail.com  
Email: vosniak@central.ntua.gr  
\*Corresponding author

**Abstract:** Geometric errors of computer numerical control (CNC) machines have a direct effect on the finished product accuracy. This paper proposes a method of correlation between position deviations of the cutting tool path in a 3-axis machine and the accuracy of part features, by example of concentricity and circularity of nominally cylindrical surfaces on a benchmark ISO test piece. The true position of the cutting tool is derived from a kinematic chain model incorporating all 21 geometric errors of the machine, fully mapped using laser doppler metrology. 16 machining tests were executed at different positions on the machine workspace. At every position circularity and concentricity of the considered features were calculated according to the kinematic model and also measured on a coordinate measuring machine (CMM). Calculated and measured accuracy values were used to train artificial neural networks as accuracy predictors.

**Keywords:** CNC; computer numerical control; geometric errors; metrology; CMM; coordinate measuring machine; CNC kinematic chains; ANNs; artificial neural networks; machining; machined test piece; laser metrology; CNC error mapping.

**Reference** to this paper should be made as follows: Koutsogiannis, M-C. and Vosniakos, G-C. (2023) 'On predicting machined part accuracy from CNC machine errors using artificial neural networks', *Int. J. Mechatronics and Manufacturing Systems*, Vol. 16, Nos. 2/3, pp.280–300.

**Biographical notes:** Marios-Christos Koutsogiannis studied Mechanical Engineering at the National Technical University of Athens from 2017 (ranking first in the entrance examination) to 2022. In parallel to his studies he worked as a Junior Manufacturing Engineer and as a Quality Inspection Engineer in the Precision Machining Industry. His research interests are in advanced mechanical design and manufacturing.

George-Christopher Vosniakos studied Mechanical Engineering at the National Technical University of Athens (1986), and obtained an MSc in Advanced Manufacturing Technology (1987) and a PhD on intelligent CAD-CAM interfaces (1991) from Univ. of Manchester (UMIST) (UK). He worked as a CIM R&D project manager in the German Software Industry, as a Lecturer at UMIST and as a Consulting Engineer. In 1999 he joined NTUA as an assistant professor advancing to professorial rank in 2015. He has been involved in over

40 R&D projects with national, European and private funding. He is a Member of the editorial board of 5 international journals and has authored over 200 publications.

## Legend

- $\delta i(i)$  Position error in direction  $i$  during movement in same direction, where  $i \in \{x, y, z\}$
- $\delta j(i)$  Straightness error in direction  $j$  during movement in direction  $i$ , where  $i, j \in \{x, y, z\} i \neq j$
- $\varepsilon i(i)$  Roll error during movement in direction  $i$ , where  $i \in \{x, y, z\}$
- $\varepsilon j(i)$  Pitch error during movement in direction  $i$ , where  $(j, i) \in \{(y, x), (z, y), (x, z)\}$
- $\varepsilon j(i)$  Yaw error during movement in direction  $i$ , where  $(j, i) \in \{(z, x), (z, y), (y, z)\}$
- $\alpha_{ij}$  Squareness error between  $i$ - $j$  axes, where  $i, j \in \{x, y, z\} i \neq j$

## 1 Introduction

Part quality in computer numerical control (CNC) machining is heavily dependent on a number of factors, including kinematic and geometrical errors of axis movement, forced vibrations or chattering, thermal phenomena and tool wear (Slocum, 1992). Each of these factors affects accuracy of the machined part, i.e., the part's smallest possible deviation from the theoretically designed shape (Orban et al., 2007). Especially in large batch production, accuracy of the CNC machine tool is critical to be tested beforehand, in order to verify that it lies within acceptable limits.

One way to verify the accuracy of the machine is through machined test parts, as defined for instance in ISO 10791. By measuring specified dimensional and geometrical tolerances the machine is deemed accurate or not (Supakumnerd and Chungchoo, 2015) without determining its errors by direct measurement. The errors of a machining process can be classified into quasi-static and dynamic. The quasi-static errors are the major source of accuracy loss and include kinematic/geometrical errors of the moving axes and thermal errors among others (Ramesh et al., 2000a). The dynamic errors describe chattering, forced vibrations and controller errors (Ramesh et al., 2000b).

In 3 axis CNC machines, there are 21 geometrical errors that affect the axis movements. Each axis has 6 errors, i.e., 3 translational  $\delta i(j)$  (linear position, horizontal straightness and vertical straightness) and 3 rotational  $\varepsilon i(j)$  (roll, pitch and yaw). Each error is defined by 2 indices,  $i$  and  $j$ , the first referring to the axis in which the error is observed and the second to the axis of movement. In addition, there are the squareness errors between the axes ( $i$  and  $j$ ) which refer to the deviation from the theoretical right angle between each pair of axes:  $\alpha_{ij}$ . The above-mentioned errors are manifested during each phase of the machining process and change the actual tool position and orientation, which results in deviations of the machined surface.

Synthesis of the 21 errors can be monitored through mathematical equations that describe the movement of the axis during machining, e.g., according to the Denavit-Hartenberg method, which focuses on the interaction of the machine's links and joints, resulting in a total homogenous transformation from the reference coordinate system to

the end point chosen (Ramos et al., 2018). This can be applied to 3 axis CNC mills up to multi-axis systems (Lin and Ehmann, 1993; Guo et al., 2020). The kinematic chain method is an alternative approach (Lee and Lin, 2012), exploiting the translational and rotational matrix between each coordinate system, from the global or reference to the workpiece coordinate system (Okafor and Ertekin, 2000). Each coordinate system is connected to the next one in the chain via homogenous transformations. For an X-Y-Z machine two kinematic chains are defined, namely the tool tip chain and the workpiece chain, both of them finally referring to the global or reference coordinate system (Soori et al., 2014).

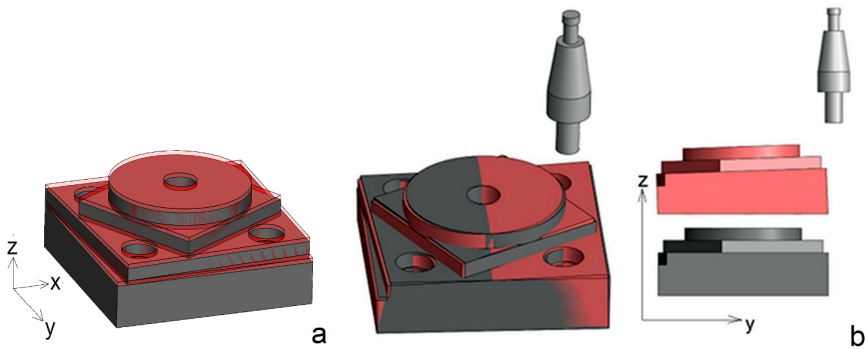
Machine tool errors are usually determined by laser interferometry, wavelength compensation being implemented according to temperature, air density and humidity (Wan et al., 2016). Error compensation is performed on the machine's controller but this relies on systematic errors that can be measured with sufficient repeatability and have a constant source (Schwenke et al., 2008). There were significant early reports on such implementations (Wu and Ni, 1989). In a semi direct method all 21 geometrical errors were defined by measurements of positional errors along 15 path lines (Chen et al., 2001). Thermal phenomena that take place during machining have been deemed necessary to incorporate in compensation procedures (Turek et al., 2010).

Correlation between machine tool errors and workpiece accuracy is relatively straightforward when a single machine error at a time is considered, see for instance Figure 1(a) and (b) where positional errors of the spindle  $\delta z(z)$  produce surfaces that are z-offset and small constant inclination of the table around X-axis resulting in inclined instead of horizontal surfaces, respectively. However, when multiple machine errors are applied, the result on the shape deviation of the machine part is not straightforward, as it requires synthesis. One of the few early attempts to such synthesis is reported in (Wilhelm et al., 1997). Subsequently, in another approach, compensated G-Code was generated for a virtual machining center incorporating 21 geometrical errors, resulting in the direct prediction of the tool movement (Soori et al., 2013). An indirect method of geometrical error compensation that is worth mentioning concerns the measurement of a test piece produced on the machine, which is then scanned into a 3D model that is imported into CAM software generating a corrected toolpath via displacement vectors compensating for deviations involved (Sortino et al., 2014). On a different line, artificial neural networks (ANNs) are used as a tool in machining metrology due to the complexity of interactions of a multitude of controllable and non-controllable parameters with the accuracy of the machine parts. A typical example of this approach used ANNs to predict the geometrical errors of a CNC machine in the whole working volume as well as cutting force errors, ultimately aiming at accuracy improvement (Raksiri and Parnichkun, 2004). Especially in the case of circular milling, as opposed to linear milling, multiple axes move at the same time. Contour milling along a continuous toolpath causes quadrant glitches and jerk movement errors due to friction in the ball screw guides (Ohashi et al., 2019). Besides, the continuous change in cutting force direction and material chip thickness has been highlighted (Deshpande et al., 2022), and a model for cutting force prediction has been developed using the toolpath and chip thickness as parameters (Wu et al., 2013). Finally, the effects of feed rate discontinuity in circular milling and how it can be avoided were studied by a regression model combined with fuzzy logic (Gassara et al., 2018). Of special importance in this context is the use of ANNs in thermal

error prediction e.g., connecting temperature with positioning deviations in CNC axes (Shi et al., 2020).

In this paper, first the machine tool's errors are fully mapped via Laser Doppler equipment. A closed form kinematic model using equations computes the displacement of the tool centre point from its nominal position for different alternative positions of the workpiece in the machine workspace. This displacement is mapped to accuracy deviations of specific workpiece features as measured on a CMM. The mapping as such is achieved by ANNs. Mapping kinematics-based calculation of tool deviations from nominal position due to machine errors in unloaded state to accuracy deviations of the machined part under machining forces became possible only by using a neural network constituting the novelty of this work. To the authors' best knowledge such an approach has not been reported so far in literature.

**Figure 1** Effect on ISO 10971 test piece of: (a) Z axis positional error and (b) X axis rotational error (see online version for colours)



Section 2 introduces kinematic models of the machine tool first by neglecting and then by considering the geometric errors of the machine tool. Section 3 describes typical procedures for measuring these geometric errors. Section 3 applies the kinematic models and uses the measured errors to compute dimensional deviations of a benchmark part by example of circularity and concentricity of two characteristic features. Section 4 presents machining of a number of identical benchmark parts at different positions of the machine workspace and measurement of circularity and concentricity of the same two characteristic features considered in the computation. Section 5 outlines the development of ANNs that predict circularity and concentricity based on the machine tool errors and the position of the part in the machine workspace. A discussion is held in Section 6 followed by a summary of conclusions and future work.

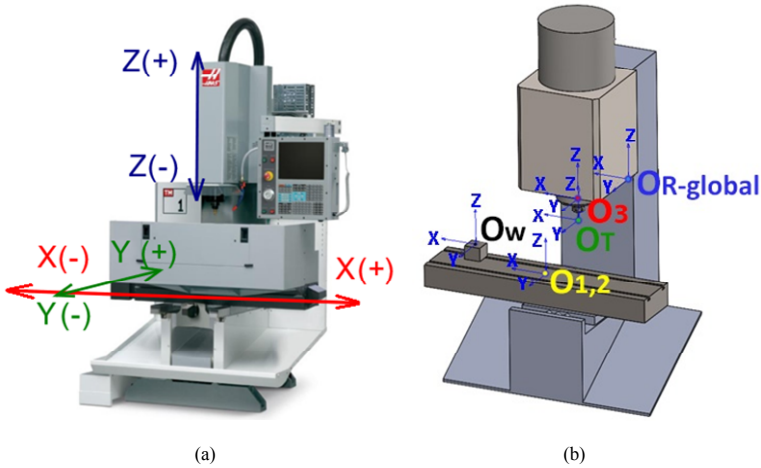
## 2 Kinematic modelling

This paper focuses, as a typical example, on the accuracy of a HAAS TM-1 3-axis vertical milling machine which comprises a bed moving in X-Y directions and a Z-moving spindle, see Figure 2(a). The following coordinate systems are defined on the machine, see Figure 2(b).

- 1 Global Reference System of the machine ( $O_{R-global}$ )
- 2 X axis coordinate system ( $O_1$ )
- 3 Y axis coordinate system ( $O_2$ )
- 4 Z axis coordinate system ( $O_3$ )
- 5 Workpiece coordinate system ( $O_W$ )
- 6 Tool-tip coordinate system ( $O_T$ ).

The global reference system is chosen to be the home position of the machine's axes (machine coordinates equal to zero on the controller). This placement is critical in order to connect the error' values (the error functions have machine coordinates as input variables, producing each error with the corresponding axis' position as input) to the corresponding position of each axis. The X and Y links coordinate systems are positioned on the centre of the machining table, while the Z link coordinate system is in the centre of the spindle tip, where the toolholder is placed and the tool coordinate system is on the centre of the tool's tip. Finally, the workpiece coordinate system is the coordinate system of the part during the programming of CAM and the origin is the one registered on the machine during the setup of the raw material.

**Figure 2** CNC mill: (a) axes and (b) coordinate systems ( $O_1, O_2, O_3$  for Z, Y, Z axis links,  $ow$  for workpiece and  $tt$  for tool tip (see online version for colours)



The machine model is based on two main kinematic chains, see Figure 3. One chain describes the connection between Machine Home Position (Reference System) to the Workpiece Coordinate System, while the other connects the tool's tip to the Machine Home Position. Each step of the chains is a homogenous transformation from the first coordinate system to the next, finally transforming the coordinates of the initial system to the reference system. The main flowchart of this method is presented in Figure 4.

**Figure 3** (a) Kinematic chains of 3 axis mill and (b) tool and workpiece actual position calculation through kinematic chains (see online version for colours)

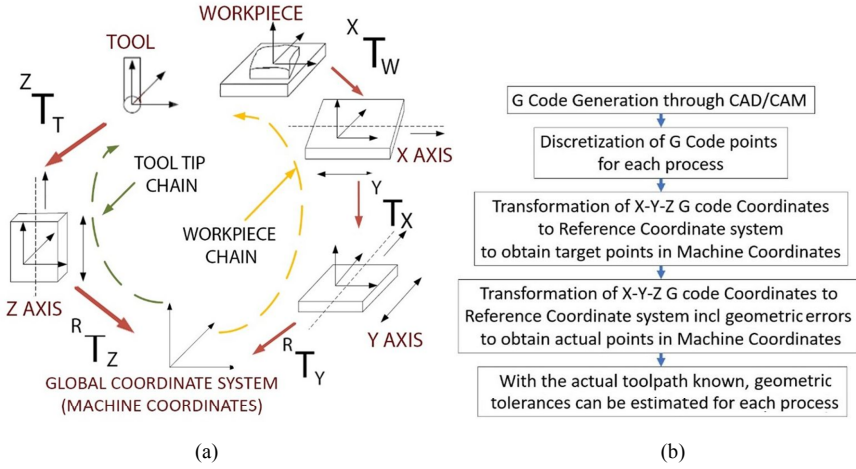
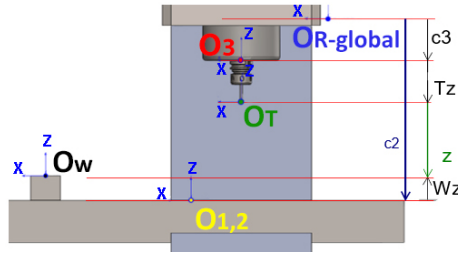


**Figure 4** Z coordinate calculation for Z system to reference system transformation  ${}^R_3T$  (see online version for colours)



### 2.1 Kinematic chain configuration neglecting machine tool errors

The kinematic chains that describe the target points, e.g., the tool tip, in machine coordinates are defined as follows. For the workpiece kinematic chain, three homogenous transformations are considered: Workpiece to X system  ${}^w_1T$ , X system to Y system  ${}^1_2T$  and Y system to Reference system  ${}^R_2T$  transformations. The final transformation is obtained by multiplying the above-mentioned matrices as follows:

$$\begin{aligned}
 {}^R_3T &= {}^R_2T \cdot {}^2_1T \cdot {}^1_0T = \begin{bmatrix} 1 & 0 & 0 & a_2 \\ 0 & 1 & 0 & y+b_2 \\ 0 & 0 & 1 & c_2 \\ 0 & 0 & 0 & 1 \end{bmatrix} \begin{bmatrix} 1 & 0 & 0 & a_1+x \\ 0 & 1 & 0 & b_1 \\ 0 & 0 & 1 & c_1 \\ 0 & 0 & 0 & 1 \end{bmatrix} \begin{bmatrix} 1 & 0 & 0 & W_x \\ 0 & 1 & 0 & W_y \\ 0 & 0 & 1 & W_z \\ 0 & 0 & 0 & 1 \end{bmatrix} \\
 &= \begin{bmatrix} 1 & 0 & 0 & W_x + a_1 + a_2 + x \\ 0 & 1 & 0 & W_y + b_1 + b_2 + y \\ 0 & 0 & 1 & W_z + c_1 + c_2 \\ 0 & 0 & 0 & 1 \end{bmatrix} \quad (1)
 \end{aligned}$$

Due to no rotation being introduced in  ${}^1_wT$ , this is simply a translational matrix, with  $W_{x-y-z}$  being the offsets in the respective axes.  ${}^2_1T$  is a translation matrix between the X and Y coordinate systems, x being the value obtained through the G code and  $a_1, b_1, c_1$  being the offsets of the X and Y systems along x-y-z axes respectively. Similarly,  ${}^R_2T$  is a translation matrix between y and reference coordinate systems, y being the value obtained through the G code and  $a_2, b_2, c_2$  being the offsets of the systems in x-y-z axes respectively, normally measured via touch probes and master gauge blocks. These 3 parameters refer to the position of the table's centre relative to the machine home position. Thus, coordinates of the target points in the global reference system (machine coordinates) are as follows:

$$x_{\text{global}} = {}^R_1T(1,4) \quad y_{\text{global}} = {}^R_1T(2,4) \quad z_{\text{global}} = {}^R_1T(3,4) \tag{2}$$

Similarly, for the tool kinematic chain, the tool tip to Z system (Spindle)  ${}^3_7T$  and Z system to Reference System  ${}^R_3T$  transformations are involved as follows:

$${}^3_7T = \begin{bmatrix} 1 & 0 & 0 & T_x \\ 0 & 1 & 0 & T_y \\ 0 & 0 & 1 & T_z \\ 0 & 0 & 0 & 1 \end{bmatrix} \quad {}^R_3T = \begin{bmatrix} 1 & 0 & 0 & a_3 \\ 0 & 1 & 0 & b_3 \\ 0 & 0 & 1 & z + c_3 \\ 0 & 0 & 0 & 1 \end{bmatrix} \tag{3}$$

where  $T_{x,y,z}$  are the tooltip's translational offsets in the Z coordinate system, while z is the target point of cutting in tool-tip coordinates, so the actual value that need to be inserted in this equation is the distance between  $O_T$  and  $O_W$  in z direction, see Figure 4.

$$z = z_{\text{Gcode}} + c_2 - c_3 + W_z - T_z \tag{4}$$

### 2.2 Kinematic chain configuration considering machine tool errors

The same principle is followed in expressing the actual position of the bed and tool tip in reference coordinate system with the major difference that the geometric errors of the machine are considered. Starting similarly from the workpiece kinematic chain,  ${}^1_wT$  remains the same as no relative motion between the workpiece and the table is present. The other two transformations in the chain are defined as follows:

$${}^2_1T = \begin{bmatrix} 1 & -\varepsilon z(x_g) & \varepsilon y(x_g) & x + \delta x(x_g) + a_1 \\ \varepsilon z(x_g) & 1 & -\varepsilon x(x_g) & \delta y(x_g) + a_{xy} \cdot x_g + b_1 \\ -\varepsilon y(x_g) & \varepsilon x(x_g) & 1 & \delta z(x_g) + a_{xz} \cdot x_g + c_1 \\ 0 & 0 & 0 & 1 \end{bmatrix}$$

$${}^R_2T = \begin{bmatrix} 1 & -\varepsilon z(y_g) & \varepsilon y(y_g) & \delta x(y_g) + a_2 \\ \varepsilon z(y_g) & 1 & -\varepsilon x(y_g) & y + \delta y(y_g) + a_{xy} \cdot y_g + b_2 \\ -\varepsilon y(y_g) & \varepsilon x(y_g) & 1 & \delta z(y_g) + a_{yz} \cdot y_{gl} + c_2 \\ 0 & 0 & 0 & 1 \end{bmatrix} \tag{5}$$

where  $x_g, y_g$  refer to the global coordinates that the machine is currently at during the machining process (live machine coordinates from the controller). The final transformation from workpiece to reference coordinate system is defined as:

$${}^R_W T = \begin{bmatrix} 1 & -\varepsilon z(y_g) - \varepsilon z(x_g) & \varepsilon y(x_g) + \varepsilon y(y_g) & \Delta_1 \\ \varepsilon z(x_g) + \varepsilon z(y_g) & 1 & -\varepsilon x(x_g) - \varepsilon x(y_g) & \Delta_2 \\ -\varepsilon y(y_g) - \varepsilon y(x_g) & \varepsilon x(x_g) + \varepsilon x(y_g) & 1 & \Delta_3 \\ 0 & 0 & 0 & 1 \end{bmatrix} \quad (6)$$

where:

$$\begin{aligned} \Delta_1 &= \alpha_1 + \alpha_2 + x + \delta x(x_g) + \delta x(y_g) + W_z \cdot [\varepsilon y(x_g) + \varepsilon y(y_g)] \\ &\quad - W_y \cdot [\varepsilon z(x_g) + \varepsilon z(y_g)] - \varepsilon z(y_g) \cdot b_1 + W_x \\ \Delta_2 &= b_1 + b_2 + y + \delta y(x_g) + \delta y(y_g) + W_x \cdot [\varepsilon z(x_g) + \varepsilon z(y_g)] \\ &\quad - W_z \cdot [\varepsilon x(x_g) + \varepsilon x(y_g)] + \alpha_{xy} \cdot y_g + \varepsilon z(y_g) \cdot (a_1 + x) + W_y \\ \Delta_3 &= c_2 + \delta z(x_g) + \delta z(y_g) + W_y \cdot [\varepsilon x(x_g) + \varepsilon x(y_g)] - W_x \cdot [\varepsilon y(x_g) + \varepsilon y(y_g)] \\ &\quad + \varepsilon x(y_g) \cdot b_1 + \alpha_{xz} \cdot x_g + \alpha_{yz} \cdot y_g - \varepsilon y(y_g) \cdot (a_1 + x) + W_z \end{aligned}$$

With the assumption that multiplication of errors which are factors of 2<sup>nd</sup> or higher order can be neglected compared to the rest of the factors. In equation (7) the focus is mainly on  $\Delta_1$  and  $\Delta_2$ , as these terms describe the actual bed position in machine coordinates, i.e., relative to reference coordinate system. The use of global coordinates in the error functions is due to the position dependence of the error value on the machine workspace and will be analysed later.

Proceeding to the tool kinematic chain a similar method is applied. The transformation matrix between the tool tip and the spindle axis  ${}^3_T$  remains constant as the only parameter that has an impact is tool length. The transformation from Z system to the reference system is given as:

$${}^R_3 T = \begin{bmatrix} 1 & -\varepsilon z(z_g) & \varepsilon y(z_g) & \delta x(z_g) + a_{xz} \cdot z + a_3 \\ \varepsilon z(z_g) & 1 & -\varepsilon x(z_g) & \delta y(z_g) + a_{yz} \cdot z + b_3 \\ -\varepsilon y(z_g) & \varepsilon x(z_g) & 1 & z + \delta z(z_g) + c_3 \\ 0 & 0 & 0 & 1 \end{bmatrix} \quad (7)$$

The error function variable is the position of the spindle during the machining process (spindle machine coordinate), and the z term is the position of the tooltip as described in the previous chapter. The final homogenous transformation is derived as:

$$\begin{aligned}
 {}^R_T T &= {}^R_3 T \cdot {}^3_T T \\
 &= \begin{bmatrix} 1 & -\varepsilon z(z_g) & \varepsilon y(z_g) & a_3 + \delta x(z_g) + T_x + T_y \cdot \varepsilon z(z_g) + T_z \cdot \varepsilon y(z_g) + \alpha_{xz} \cdot z_g \\ \varepsilon z(z_g) & 1 & -\varepsilon x(z_g) & b_3 + \delta y(z_g) + T_y + T_x \cdot \varepsilon z(z_g) + T_z \cdot \varepsilon x(z_g) + \alpha_{yz} \cdot z_g \\ -\varepsilon y(z_g) & \varepsilon x(z_g) & 1 & c_3 + z + \delta z(z_g) + T_z + T_x \cdot \varepsilon y(z_g) + T_y \cdot \varepsilon x(z_g) \\ 0 & 0 & 0 & 1 \end{bmatrix}
 \end{aligned} \tag{8}$$

From the above the conclusion is that the actual position of the tool’s tip is derived from the term  ${}^R_T T(3,4)$  and taking into account the terms  ${}^R_W T(1,4)$ ,  ${}^R_T T(2,4)$ , a fully defined actual position can be derived in machine coordinates. These 3 terms will be used to analyse circularity and concentricity of the machined test part during the machining experiments that follow.

### 3 Machine tool geometric error measurement

Position, straightness, orientation (yaw, pitch, roll angles) as well as squareness errors were measured employing the Optodyne™ Laser Doppler Displacement Meter type MCV-500; straightness and squareness measurement involved additional optical kits consisting of a quad detector and optical square. It consists of the laser source which emits the beam, the retroreflector which serves as a reflecting target for the beam, the processor module which provides power to the unit and includes the processor that translates the analogue laser signal to digital data forwarded to the connected PC. The squareness-straightness equipment also includes the quad detector, a device with 4 photodetectors, with the ability to pinpoint the exact point of the laser beam on its surface, as well as the optical square, a penta-prism with the ability to bend the laser beam to 90° with a tolerance of 2–5 arcsec. The accuracy of the LDDM measuring system is stated as 1 ppm, with automatic temperature compensation via air and table temperature sensors. The maximum length measured was the 800 mm of the X axis travel, hence all linear displacement measurements are of sub-micron accuracy.

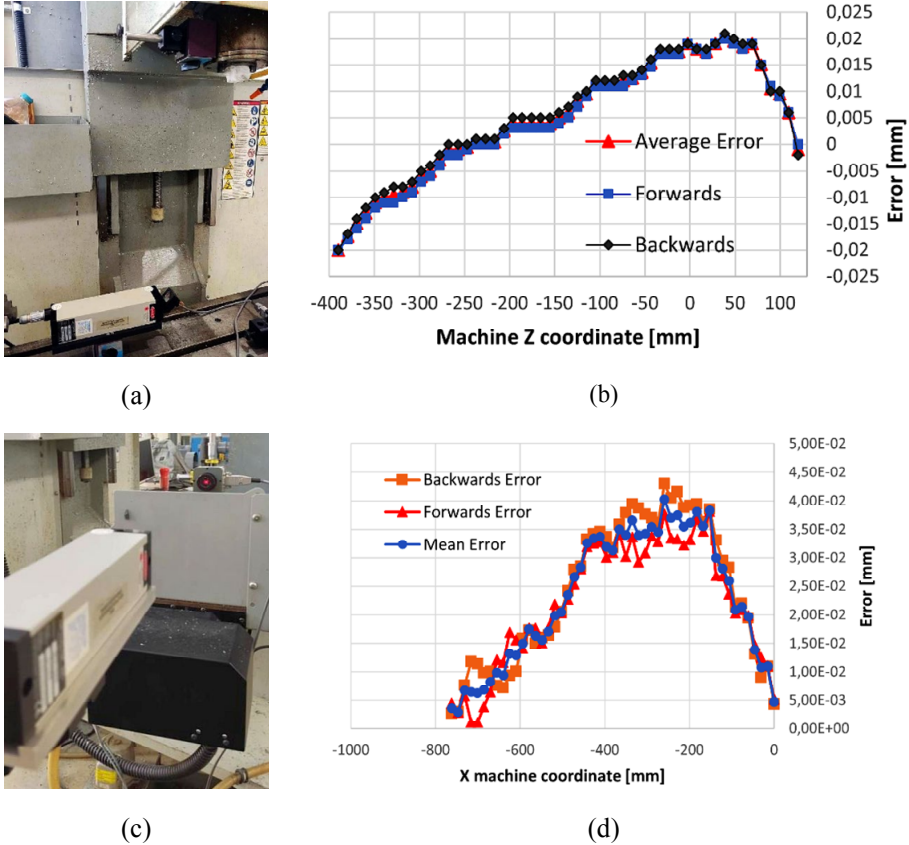
Positioning errors  $\delta x(x)$ ,  $\delta y(y)$  and  $\delta z(z)$  were computed automatically by the Optodyne™ software according to ISO 230-2: 2012. For instance, in order to determine positioning error  $\delta z(z)$ , see layout in Figure 5(a) Z-axis travel range from –390 to 120 mm was scanned by automatically constructing G-code for Z movement using a step of 10.2 mm in both forwards and backwards direction resulting in an indicative error map of Figure 5(b). Straightness errors are measured by employing a quad detector recording deviation of the laser beam from its centre, in a direction parallel to the planar movement of the axis (horizontal straightness) or perpendicular to it (vertical straightness). For example, the layout for  $\delta(x)$  is shown in Figure 5(c) and the error map in Figure 5(d).

The pitch and yaw errors for each axis were measured indirectly by utilising the Abbé error theory suggesting that the angular error can be calculated if two linear measurements with known offset are made along the axis. For example, measurement of pitch error  $\varepsilon y(x)$  and yaw error  $\varepsilon z(y)$  is shown in Figure 6. The error is calculated in the whole travel range of x axis as:

$$\varepsilon_y(x) = \operatorname{atan} \left( \frac{\operatorname{avg}(\delta x(x)_1) - \operatorname{avg}(\delta x(x)_2)}{R_1 - R_2} \right) \quad (9)$$

where  $\operatorname{avg}(\delta x(x))$  is the average error of forwards and backwards linear positioning error of the x axis at each x value, and indices 1–2 refer to the respective set of measurements, while  $R_1$  and  $R_2$  are the Abbé offsets.

**Figure 5** Measurement of positioning error  $\delta z(z)$  ((a) layout and (b) mapping) and straightness error  $\delta z(x)$  ((c) layout and (d) mapping) (see online version for colours)



Similarly, to calculate yaw error  $\varepsilon_z(y)$ , with Abbé offsets known through the distance of the reflective mirror positions  $R$ , see Figure 6(e), measurements of the positioning error  $\delta y(y)$  were taken through y axis travel, yielding:

$$\varepsilon_z(y) = \operatorname{atan} \left( \frac{\operatorname{avg}(\delta y(y)_1) - \operatorname{avg}(\delta y(y)_2)}{R} \right) \quad (10)$$

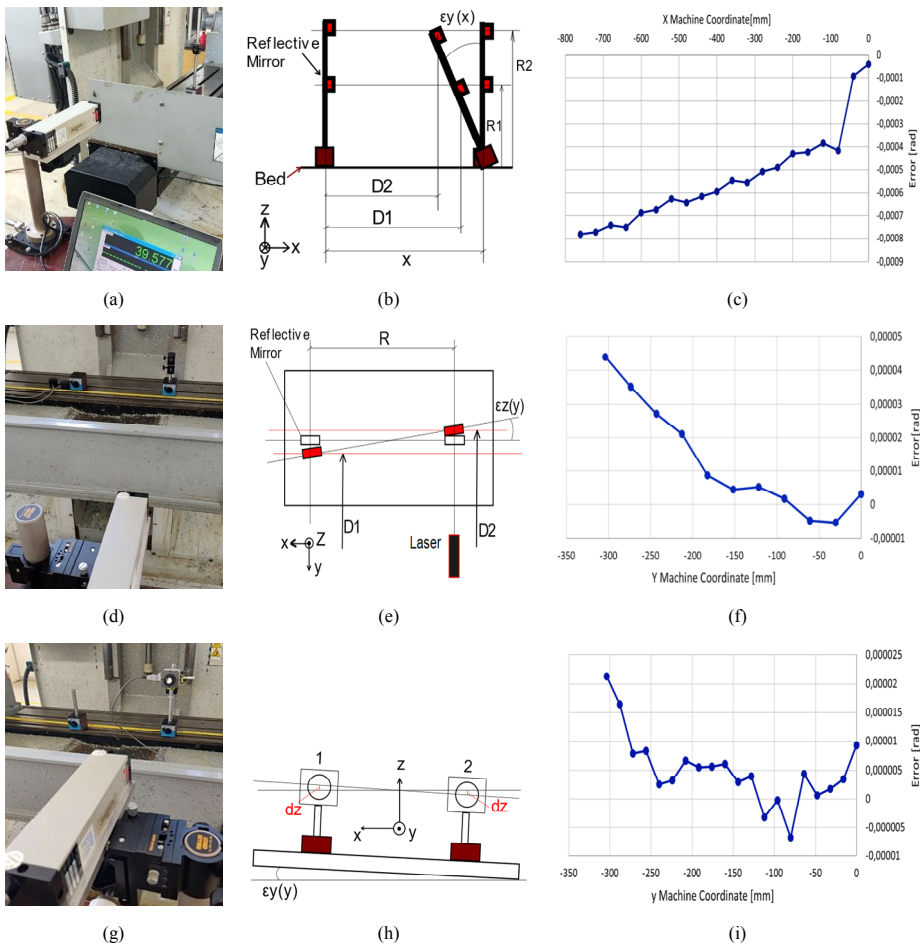
Determining roll errors presented the challenge of using the Quad Detector to monitor changes in the inclination of the associated moving member of the machine structure, see Figure 6(g). Using  $\varepsilon_y(y)$  as an example, as the table rotates by small angles around Y axis

during movement of Y axis, deviations in the Z direction can be observed. For each position of the Y axis, the deviation in Z axis can be recorded through a Quad Detector, in two different positions in the X axis in order to calculate the respective angle of rotation see Figure 6(h). The distance between the two measurement positions is known, as well as dz deviations thus roll error can be calculated as:

$$\epsilon_y(y) = \text{atan} \left( \frac{\text{avg}(dz_2) - \text{avg}(dz_1)}{R} \right) \tag{11}$$

The corresponding variation of inclination for the full Y axis travel is shown in Figure 6(i).

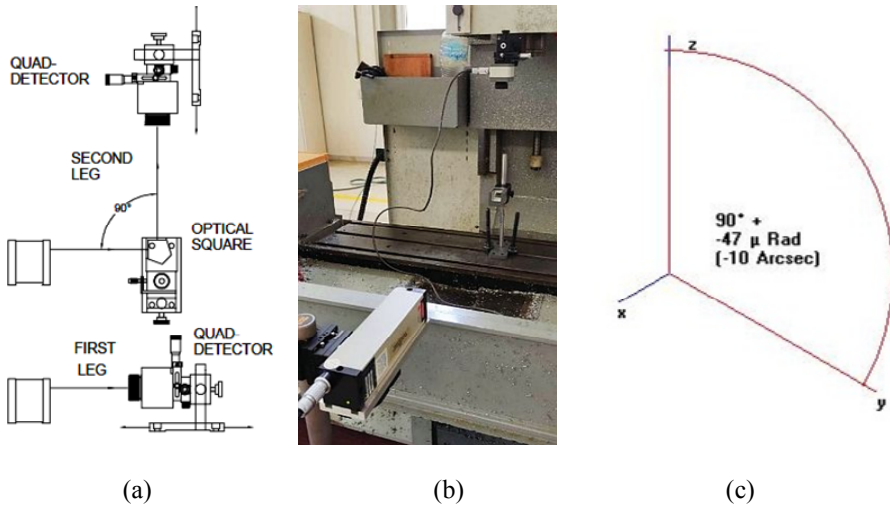
**Figure 6** Layout, calculation parameters and results of measurement of errors pitch  $\epsilon_y(x)$  (a, b, c), yaw  $\epsilon_z(y)$  (d, e, f) and roll  $\epsilon_y(y)$  (g, h, i) (see online version for colours)



Finally, determining squareness error of each pair of axes requires both a quad detector and an optical square. The measurement principle is that firstly, a reference beam is calibrated parallel to the first axis of measurement, through successive straightness

measurements in the direction of this axis. With the beam kept steady and perfectly parallel to the reference axis, the optical square is introduced at the end of the reference beam, bending it precisely at  $90^\circ$ , in order to create the second beam of the perpendicular axis, through a second series of successive straightness measurements in the perpendicular beam. In each series of measurements, the laser source is kept steady. The moving component is the quad detector. With the first and second leg of the angle correctly defined, the Optodyne™ software calculates the true angle between the two reference beams, resulting in the squareness error between the two axes. Figure 7 depicts the principle, layout and result of Y-Z squareness of the CNC milling machine at hand.

**Figure 7** Squareness measurement: (a) method; (b) layout for Y-Z squareness and (c) result presentation (see online version for colours)



#### 4 Part feature dimension calculation based on measured machine tool errors

The part to be machined is a benchmark workpiece specified in ISO 10791:2014 M1. The material was Al 2024. For demonstration purposes in the rest of this paper two particular features at the top section of the part are concentrated on, namely the external cylinder surface and the concentric hole, see Figure 8.

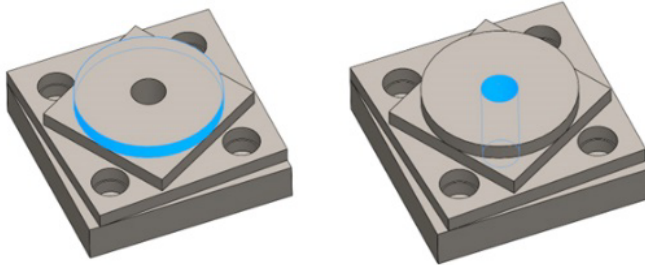
##### 4.1 Circularity of external cylindrical surface sections

Circularity is normally achieved by the final finish machining pass. The tool centre path is a circle (circular interpolation) of diameter  $\varnothing 59\text{mm}$ . This circle is discretised into 21 points with known coordinates as given to the machine controller by the G-code. The aim is to transform these coordinates into machine coordinates through the actual  ${}^R_w T$  homogenous transformation which includes the geometric errors. The X and Y coordinates of the tool centre are derived as:

$$\begin{aligned}
 {}^R_wT(1,4) &= A_1 = \alpha_1 + \alpha_2 + x + \delta x(x_g) + \delta x(y_g) + W_z \cdot [\varepsilon y(x_g) + \varepsilon y(y_g)] \\
 &\quad - W_y \cdot [\varepsilon z(x_g) + \varepsilon z(y_g)] - \varepsilon z(y_g) \cdot b_1 + W_x \\
 {}^R_wT(2,4) &= A_2 = b_1 + b_2 + y + \delta y(x_g) + \delta y(y_g) + W_x \cdot [\varepsilon z(x_g) + \varepsilon z(y_g)] \\
 &\quad - W_z \cdot [\varepsilon x(x_g) + \varepsilon x(y_g)] + \alpha_{xy} \cdot (x_g + y_g) + \varepsilon z(y_g) \cdot (a_1 + x) + W_y
 \end{aligned} \tag{12}$$

According to the machining approach followed, the tool does move in the Z direction only stepwise, thus circularity is affected only by the table movement in X-Y plane. The tool’s kinematic chain provides information for the final depth of the machined cylinder by the homogenous transformation element  ${}^R_1T(3,4)$ . Equation (13) suggest a position error of the whole circular path and a circularity error.

**Figure 8** Machined test part highlighted surface features of interest (see online version for colours)

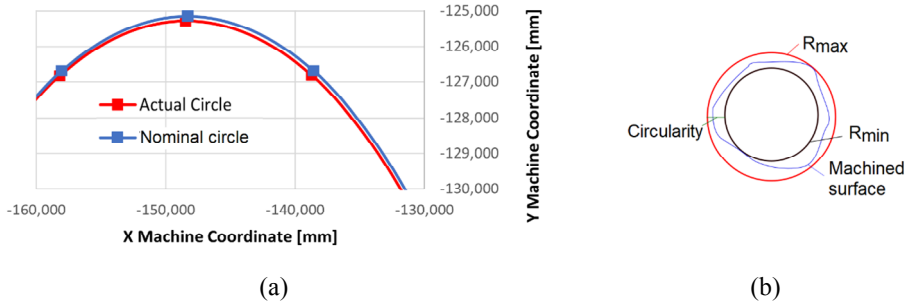


Circularity is defined as the difference in radii of two concentric circles with minimum radius difference, between which the actual surface of the part lies (Krulikowski, 2012), see Figure 9(a). Considering the total  $i = 1, \dots, 21$  points in machine coordinates, the radii of the two concentric circles are calculated as follows:

$$\begin{aligned}
 R_{min}^2 &= \text{minimum} \left[ (x_i^2 - x_{ci}^2) + (y_i^2 - y_{ci}^2) \right] R_{max}^2 \\
 &= \text{maximum} \left[ (x_i^2 - x_{ci}^2) + (y_i^2 - y_{ci}^2) \right] \text{ for all } i
 \end{aligned} \tag{13}$$

where  $x_i$  and  $y_i$  are the true coordinates of the tool centre point  $i$  following the circular interpolation, while  $x_{ci}$  and  $y_{ci}$  are the coordinates of the true centre of the circular interpolation ( $x = 0, y = 0$ ), transformed into machine coordinates through  ${}^R_wT$  homogenous transformation that includes the geometric errors. Thus, for each point of the circular interpolation, the distance from the actual centre of the interpolation is calculated to enable searching for the minimum and maximum distance and then calculation of circularity.

**Figure 9** (a) Deviations between commanded and actual points of circular toolpath and (b) circularity definition (see online version for colours)



#### 4.2 Concentricity

Concentricity between the external cylindrical surface ( $\varnothing 55$ ) and the hole ( $\varnothing 13$ ) of the test piece, see Figure 8, is studied by first calculating the drill’s true centre. This is the result of two parameters. The first is the table position error before the start of the drilling cycle. The second parameter is the drill’s deviation in the X-Y plane during its movement in the Z axis. This results from combining the straightness and squareness errors during the spindle’s vertical motion. Thus, the drill centre is shifted as it proceeds to the maximum depth. Again, discretisation of the tool path is necessary; the drill’s position is calculated in 1 mm steps along the drilling depth, i.e., from  $Z = 0$  to  $Z = -10$  mm in workpiece coordinates.

Firstly, the positioning error of the table is calculated when it is called to approach the position  $[0,0]$  in the X-Y plane. This has already been covered in the circularity section ( $x_{Table} = {}^R T(1,4)$  και  $y_{Table} = {}^R T(2,4)$  see equation (13) with  $x = y = 0$ ). A least-squares circle is fitted to the actual circle points calculated above yielding its centre  $[x_c, y_c]$  and diameter. The tool’s kinematic chain is necessary to calculate deviation. Specifically, the elements  $x_{dev} = {}^R T(1,4)$ ,  $y_{dev} = {}^R T(2,4)$  are extracted, while the term  ${}^R T(3,4)$  describes the actual drilling depth. The actual position of the drill at each Z-step in machine coordinates is calculated as the algebraic sum:

$$x_{drill} = x_{Table} + {}^R T(1,4) \quad y_{drill} = y_{Table} + {}^R T(2,4) \tag{14}$$

So, the concentricity can be calculated as:

$$Concentricity = \sqrt{(average[x_{drill}] - x_c)^2 + (average[y_{drill}] - y_c)^2} \tag{15}$$

### 5 Part machining and feature dimension measurement

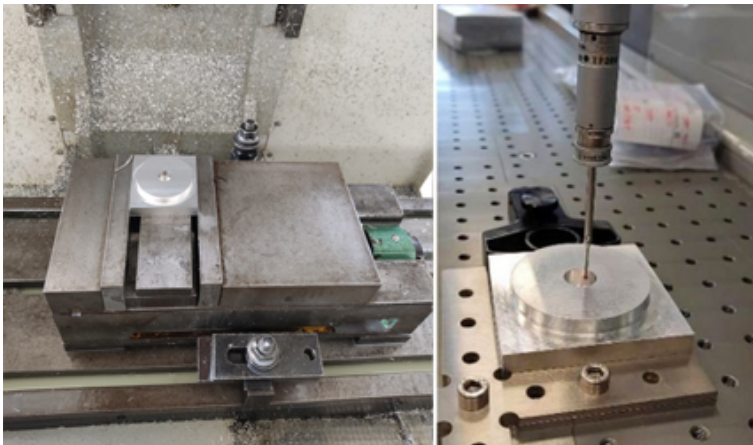
For the machining process, a large number of roughing passes was chosen in order to mitigate the effect of cutting forces on the final geometry, cutting conditions being sufficiently conservative. A final radial pass of  $50 \mu\text{m}$  depth was employed for the external cylindrical surface using a  $\varnothing 8$  mm 3-flute side mill (KORLOY APFE3080-060) at a feed of  $400 \text{ mm/min}$  and a spindle speed of  $3800 \text{ rpm}$ . The  $\varnothing 13$  hole was created

using a  $\varnothing 13$  mm solid carbide TiAlN coated drill (INNOVA 303.130.00) at a feed of 20 mm/min and a spindle speed of 3800 rpm. Another important factor of the machining process is the thermal warm-up of the machine, due to various thermal losses occurring during the machining in the spindle's bearings, the ball-screws of the axes and the feed motors (Wenkler et al., 2022). Additionally, the above-mentioned measurements are affected by the ambient temperature, which has an effect on the error mapping, especially on linear errors and less so on rotational errors (Groos et al., 2020). The ambient temperature throughout the error mapping was monitored at 24–25°C. The warm-up sequence used in order to minimise the thermal drift due to axis motion and spindle rotations is the one proposed in the machine's manual, involving successive increase steps in the spindle's rotational speed for 20 min duration, as well as rapid and slow motion of the 3 axes during this time with G0 and G1 commands.

16 identical parts were machined, corresponding to 16 different locations on the table, using a workholding vice to keep the raw material steady. The vice was placed in different locations, changing the origin point of the part in all 3 coordinates, see Figure 10. Due to the shape and size of the bed, machining location range on X axis ranged from –125 mm to –634 mm, while the Y axis locations ranged from –103 mm to –195 mm due to space restrictions of the workholding vice and Z-axis levels ranged from –242 mm to –322 mm with the help of parallel gauge blocks. For each machined part and respective unique location in the machine's workspace, the setup origin point was recorded (X-Y-Z Machine Offsets), as well as the tool length of each process. This data was used as input for the kinematic chains in order to calculate the circularity and concentricity as analysed in Section 4.

Circularity and concentricity of the cylinder and hole features respectively, that were calculated in Section 4, were also measured on a DEA Scirocco™ Coordinate Measurement Machine by BROWN & SHARPE possessing an accuracy of  $2.8+4L/1000$   $\mu\text{m}$ , see Figure 10.

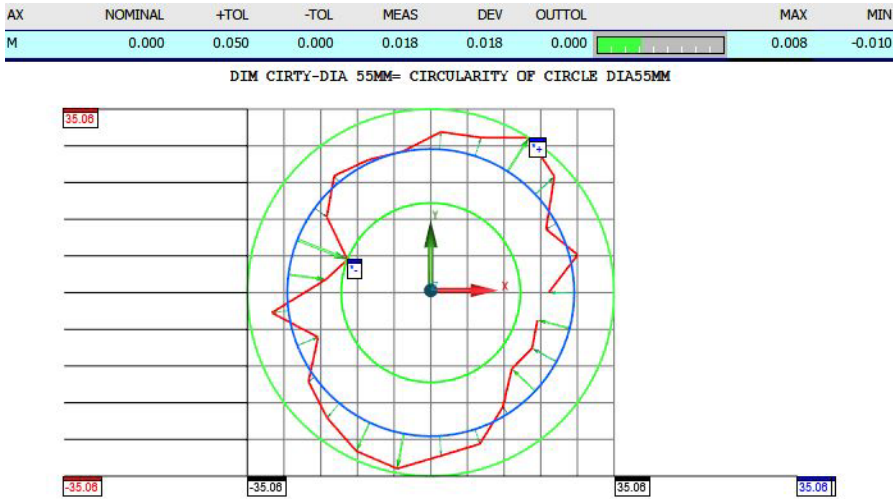
**Figure 10** Part machining setup (left) and part measurement setup (right) (see online version for colours)



The Renishaw™ PH10M Plus head was used, along with a TP200 touch probe and a  $\varnothing 2$  mm Mitutoyo™ stylus tip. The CMM was programmed through PC-DMIS 2021. In order to scan the circular section of the external cylindrical surface, 21 hit points were

measured at a depth of  $Z = -3$  mm from the top plane of the part due to the size of the stylus tip. As far as hole is concerned, 3 depth levels were chosen, with 5 hit points at each level and a pitch of 1 mm in order to scan most of the hole’s surface. A typical circularity polar plot can be observed in Figure 11. The red line connects the measured points, the green arrows showing the direction of deviation from the nominal blue circle. The two green circles represent the minimum and maximum diameters that can be fitted to the measured data, hence calculating the test piece circularity.

**Figure 11** Polar plot of circularity for test piece no 13 (see online version for colours)



## 6 Predictive artificial neural networks

It is hypothesised that differences between calculated values of circularity or concentricity and actual ones measured by CMM on the machined part are attributed to the fact that, by definition, the former neglect machining forces since the kinematic chain transformations refer to no load condition. Furthermore, these differences as depicted in Figure 12 vary for the different locations of the part on the machine table, since each test piece number corresponds to a different location in the machine’s workspace. Thus, it is reasonable to assume that knowledge of the part location on the table is necessary in order to determine the difference of the actual circularity or concentricity of the respective features from the theoretical ones calculated for no-load condition. The values of circularity and concentricity obtained via the kinematic chain model and the CMM measurements can be observed in Table 1.

Therefore, the calculated and measured circularity datasets, see Figure 12(a), were used in order to train an ANN in order to generalise their correlation into a circularity prediction tool. Similarly, a concentricity prediction ANN was constructed from the respective calculated and measured concentricity datasets, whose differences are shown in Figure 12(b). Both ANNs were simple feedforward backpropagation multiple layer perceptrons and were implemented on Matlab™ using the inbuilt shallow neural network library.

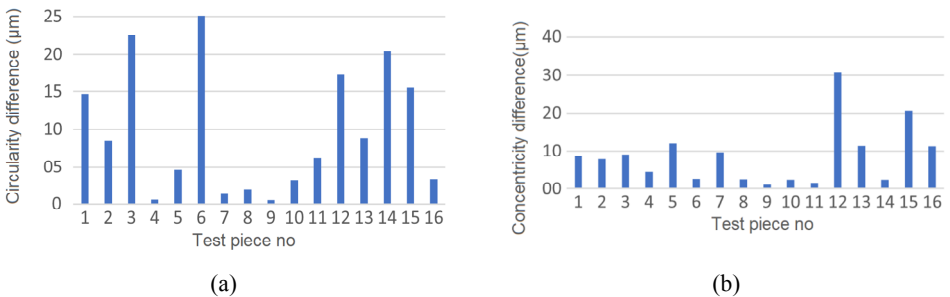
The circularity ANN was designed with four inputs, i.e., the X, Y, Z machine coordinates of the part’s origin (stored as axis offsets in the machine controller during the setup process of the part), as well as the calculated circularity in this specific position in the machine work volume, see Section 4. Its output is the actual circularity of the part’s feature.

Numerous ANN architectures were tried and tested, using a brute force enumeration approach. This involved trying one or two hidden layers and 3–10 neurons per layer, aiming at the optimum performance as quantified by the mean absolute error (MAE) between predicted and targeted circularity values for both the training and the testing dataset. The best architecture proved to include 2 hidden layers with 4 and 3 neurons respectively.

**Table 1** Calculated and measured circularity and concentricity data

Test piece	Circularity [mm]			Test piece	Concentricity [mm]		
	Kinematic chain calculation	Measured	Deviation		Kinematic chain calculation	Measured	Deviation
1	0.016	0.031	0.015	1	0.033	0.024	0.009
2	0.022	0.013	0.009	2	0.021	0.029	0.008
3	0.036	0.013	0.023	3	0.036	0.027	0.009
4	0.015	0.016	0.001	4	0.022	0.017	0.005
5	0.023	0.018	0.005	5	0.018	0.03	0.012
6	0.038	0.013	0.025	6	0.032	0.029	0.003
7	0.021	0.020	0.001	7	0.037	0.027	0.010
8	0.025	0.027	0.002	8	0.023	0.02	0.003
9	0.017	0.016	0.001	9	0.025	0.024	0.001
10	0.019	0.022	0.003	10	0.026	0.028	0.002
11	0.022	0.016	0.006	11	0.03	0.028	0.002
12	0.026	0.009	0.017	12	0.013	0.044	0.031
13	0.027	0.018	0.009	13	0.043	0.032	0.011
14	0.036	0.016	0.02	14	0.03	0.028	0.002
15	0.026	0.010	0.016	15	0.026	0.047	0.021
16	0.017	0.020	0.003	16	0.032	0.043	0.011

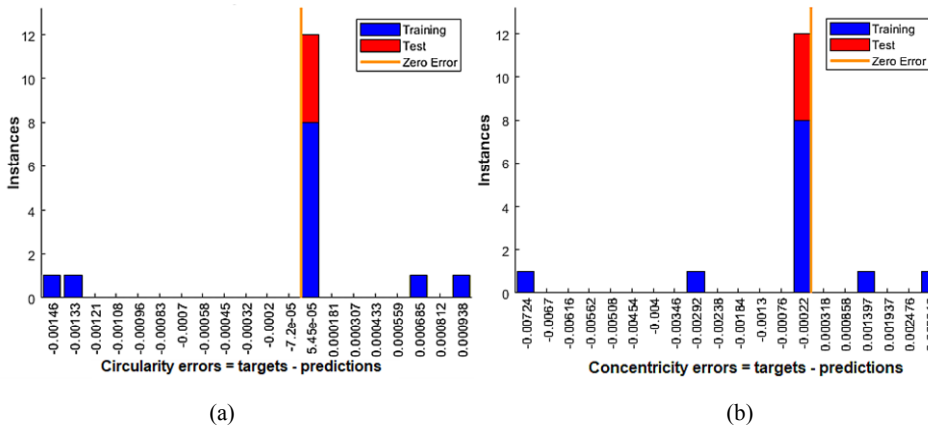
**Figure 12** Difference between measured and calculated: (a) circularity and (b) concentricity (see online version for colours)



Training was achieved through K fold method of data separation, creating 4 different data subsets of the 16 values of circularity. These is a small dataset indeed, highlighting the fact that very often, as in this case, too, it is too expensive to generate large datasets to train ANNs. The training algorithm chosen was Levenberg-Marquardt. For each fold, the weights were used as initialisation for the next fold, resulting in gradual improvement of the network’s performance. The stopping conditions of the training were a testing correlation factor ( $R^2$ ) higher than 0.98 and a MAE value lower than 2.5  $\mu\text{m}$ .

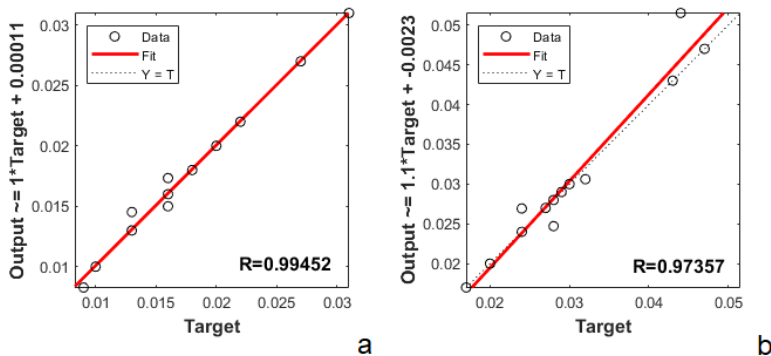
The ANN’s performance was acceptable, since MAE was under 0.2  $\mu\text{m}$  and the error histogram revolved around 0 $\mu\text{m}$ , see Figure 12(a).  $R^2$  coefficient for both training and testing data was high, see Figure 13(a).

**Figure 13** ANN error histograms of: (a) circularity and (b) concentricity (see online version for colours)



The concentricity ANN was created similarly, inputs being the part origin X-Y-Z offsets and the kinematically calculated concentricity. The ANN output is the actual concentricity, as measured via the CMM. The best architecture of the ones tried was identical to that of the circularity ANN, i.e., two hidden layers with 4 and 3 neurons respectively. Performance of this ANN was also acceptable, see Figure 13(b). Correlation coefficient for both training and testing data was high, see Figure 14(b).

**Figure 14** ANN bundled training and testing correlation coefficients for: (a) circularity and (b) concentricity (see online version for colours)



## 7 Conclusions

In this study, an innovative connection between kinematic modelling of machine tool errors and workpiece metrology was achieved through ANNs.

- The use of laser equipment kinematic error mapping in a 3 axis CNC machine allows direct measurement of positioning, straightness and squareness errors, whereas yaw, pitch and roll angular errors were measured indirectly avoiding the need for special equipment.
- The ANNs provided the transformation from kinematically calculated tool path errors under no load conditions to actual errors of the part features in the presence of machine forces, with good prediction capability at least for circularity and concentricity of designated part features.
- Such ANNs can be used to determine by trial-and-error acceptable position for part setup inside the machine workspace, which is especially useful for machines with reduced accuracy. They can also be used for pre-machining evaluation of the resulting part accuracy in order to verify that the finished product will lie within the stated tolerance zones before production starts.
- Geometric and dimensional deviations of a surface feature, such as plane, cylinder etc., for a given machine tool come down to the positioning errors of the cutting tool edges that create these features, as well as the position and orientation of these features in the machine workspace. The kinematic chain method employed does provide the capability to calculate the deviated tool edges due to geometric errors captured in the chain. However, these surface features are generated as an envelope of successive positions of the cutting tool edges, which was not done in this study, since it requires solid modelling operations typically implemented in CAM software. Instead, the deviated path of the tool centre point was determined and was deemed representative enough to be correlated with the measured deviations of the machined features, in this case concentricity and circularity.

The same approach and tools can be readily applied to determining accuracy of other features, e.g., flatness of planar surfaces, parallelism of planes etc. This is an immediate next step to further validate the methodology. A further step in this research is to generalise it so as to become independent of the position and orientation of features which is possible, since all features consist of points which undergo deviations that are in the first phase calculated using the kinematic chain error budgeting principle and, in a second phase, they are corrected by comparison to real measurements capturing process and machine dynamics, too.

Limitations pertain notably to the omission of dynamic and thermal errors. An effort to mitigate these phenomena was made, with conservative cutting conditions and constant coolant flow on the cutting edge, which had no previous wear, but the model would need to include these parameters in order to produce more accurate results. The mapping process also has limitations, as measurements cannot be made at infinitely small intervals along CNC machine axes.

## References

- Chen, G., Yuan, J. and Ni, J. (2001) 'A displacement measurement approach for machine geometric error assessment', *International Journal of Machine Tools and Manufacture*, Vol. 41, No. 1, pp.149–161.
- Deshpande, S., Araujo, A.C., Lagarrigue, P. and Landon, Y. (2022) 'Experimental analysis of circular milling for material identification in aerospace industry', *Key Engineering Materials*, Vol. 926, pp.1650–1659, Trans Tech Publications Ltd.
- Gassara, B., Baili, M., Dessein, G., Hbaieb, M. and Saï, W.B. (2013) 'Feed rate modeling in circular–circular interpolation discontinuity for high-speed milling', *The International Journal of Advanced Manufacturing Technology*, Vol. 65, pp.1619–1634.
- Groos, L., Held, C., Keller, F., Wendt, K., Franke, M. and Gerwien, N. (2020) 'Mapping and compensation of geometric errors of a machine tool at different constant ambient temperatures', *Precision Engineering*, Vol. 63, pp.10–17.
- Guo, H., Yang, X., Wang, S. and Dai, Z. (2020) 'Research on the application of multiplication dimension reduction method in global sensitivity analysis of CNC machine tools', *AIP Advances*, Vol. 10, No. 1, p.015029.
- Krulikowski, A. (2012) *Fundamentals of Geometric Dimensioning and Tolerancing*, Cengage Learning.
- Lee, R.S. and Lin, Y.H. (2012) 'Applying bidirectional kinematics to assembly error analysis for five-axis machine tools with general orthogonal configuration', *The International Journal of Advanced Manufacturing Technology*, Vol. 62, pp.1261–1272.
- Lin, P.D. and Ehmman, K.F. (1993) 'Direct volumetric error evaluation for multi-axis machines', *International Journal of Machine Tools and Manufacture*, Vol. 33, No. 5, pp.675–693.
- Ohashi, T., Shibata, H., Futami, S. and Sato, R. (2019) 'Quadrant glitch compensation by a modified disturbance observer for linear motor stages', *Precision Engineering*, Vol. 59, pp.18–25.
- Okafor, A.C. and Ertekin, Y.M. (2000) 'Derivation of machine tool error models and error compensation procedure for three axes vertical machining center using rigid body kinematics', *International Journal of Machine Tools and Manufacture*, Vol. 40, No. 8, pp.1199–1213.
- Orban, P.E., Yeung, M., Jiang, Y. and Jiang, J. (2007) 'Machining error correction at batch processing', *SAE Transactions*, Vol. 116, No. 5, pp.271–277.
- Raksiri, C. and Parnichkun, M. (2004) 'Geometric and force errors compensation in a 3-axis CNC milling machine', *International Journal of Machine Tools and Manufacture*, Vol. 4, Nos. 12–13, pp.1283–1291.
- Ramesh, R., Mannan, M.A. and Poo, A.N. (2000a) 'Error compensation in machine tools—a review: part I: geometric, cutting-force induced and fixture-dependent errors', *International Journal of Machine Tools and Manufacture*, Vol. 40, No. 9, pp.1235–1256.
- Ramesh, R., Mannan, M.A. and Poo, A.N. (2000b) 'Error compensation in machine tools—a review: part II: thermal errors', *International Journal of Machine Tools and Manufacture*, Vol. 40, No. 9, pp.1257–1284.
- Ramos, P.B., Medina, J.M., Salcedo, M.C., Peña, A.R. and Ochoa, G.V. (2018) 'Application of the Denavit-Hartenberg method to estimate the positioning errors of an automated XYZ Cartesian table', *Contemp Eng Sci.*, Vol. 11, pp.3483–3493.
- Schwenke, H., Knapp, W., Haitjema, H., Weckenmann, A., Schmitt, R. and Delbressine, F. (2008) 'Geometric error measurement and compensation of machines—an update', *CIRP Annals*, Vol. 57, No. 2, pp.660–675.
- Shi, H., Jiang, C., Yan, Z., Tao, T. and Mei, X. (2020) 'Bayesian neural network–based thermal error modeling of feed drive system of CNC machine tool', *The International Journal of Advanced Manufacturing Technology*, Vol. 108, pp.3031–3044.
- Slocum, A.H. (1992) *Precision Machine Design*, Society of Manufacturing Engineers.

- Soori, M., Arezoo, B. and Habibi, M. (2014) 'Virtual machining considering dimensional, geometrical and tool deflection errors in three-axis CNC milling machines', *Journal of Manufacturing Systems*, Vol. 33, No. 4, pp.498–507.
- Soori, M., Arezoo, B. and Habibi, M. (2013) 'Dimensional and geometrical errors of three-axis CNC milling machines in a virtual machining system', *Computer-Aided Design*, Vol. 45, No. 11, pp.1306–1313.
- Sortino, M., Belfio, S., Motyl, B. and Totis, G. (2014) 'Compensation of geometrical errors of CAM/CNC machined parts by means of 3D workpiece model adaptation', *Computer-Aided Design*, Vol. 48, pp.28–38.
- Supakumnerd, K. and Chungchoo, C. (2015) 'An application of finished test piece methods for evaluating the performance of computer numerical control machining and turning centers', *Agriculture and Natural Resources*, Vol. 49, No. 6, pp.951–962.
- Turek, P., Jędrzejewski, J. and Modrzycki, W. (2010) 'Methods of machine tool error compensation', *Journal of Machine Engineering*, Vol. 10, No. 4, pp.5–25.
- Wan, M., Liu, Y. and Zhang, W. (2016) 'A new algorithm for the identification of CNC geometric errors', *Procedia CIRP*, Vol. 56, pp.293–298.
- Wenkler, E., Selch, M., Hellmich, A. and Ihlenfeldt, S. (2022) 'Process concatenation to reduce thermal changes in machine tools', *International Journal of Mechatronics and Manufacturing Systems*, Vol. 15, Nos. 2–3, pp.167–184.
- Wilhelm, R.G., Srinivasan, N., Farabaugh, F. and Hocken, R. (1997) 'Part form errors predicted from machine tool performance measurements', *CIRP Annals*, Vol. 46, No. 1, pp.471–474.
- Wu, B., Yan, X., Luo, M. and Gao, G. (2013) 'Cutting force prediction for circular end milling process', *Chinese Journal of Aeronautics*, Vol. 26, No. 4, pp.1057–1063.
- Wu, S.M. and Ni, J. (1989) 'Precision machining without precise machinery', *CIRP Annals*, Vol. 38, No. 1, pp.533–536.